Overpressuring mechanisms in the Yinggehai Basin, South China Sea

Xiaorong Luo, Weiliang Dong, Jihai Yang, and Wan Yang

ABSTRACT

Yinggehai Basin is an elongate Cenozoic rift basin on the northwestern margin of the South China Sea continental shelf. Its thick (~17 km) basin fill is characterized by high geothermal gradient and high overpressure. Overpressure associated with nonequilibrium compaction mainly occurs at depths more than 2800 m at the basin center and more than 4000 m at the basin margin because the shallow-buried Neogene and Quaternary strata lack effective seals. This regional overpressure distribution, however, is disrupted at basin center where high overpressure occurs in permeable formations at a depth as shallow as 1400 m on top of a series of deep-seated faults and fractures. We studied the processes and mechanisms of overpressuring via numerical modeling that couples basin filling, sediment compaction, and thermal and pressure fields to approach the origin of the shallow high overpressure. Model results indicated that an increase of fluid volume due to natural-gas generation by organic cracking is not large enough to generate the overpressure because of the limited amount of organic matter. The shallow overpressure has probably been generated allogenically. Deep open faults have served as vertical hydraulic conduits and channeled the deep high pressure into shallow permeable formations.

INTRODUCTION

Overpressures are common in sedimentary basins (Fertl, 1976) and have been intensively studied in geophysics (Bethke, 1986) and geodynamics (Turcotte and Schubert, 1982). Many overpressuring mechanisms (Smith, 1971; Fertl, 1976; Magara, 1978; Osborne and Swarbrick, 1997) can adequately explain the overpressure formation in low-permeability argillaceous formations. It is generally considered that overpressures within permeable formations resulted from transmission of fluid and pressure from adjacent low-permeability formations (Fertl, 1976; Magara, 1978). In this case, the pressures in

Manuscript received November 7, 2001; provisional acceptance May 15, 2002; revised manuscript received July 23, 2002; final acceptance October 17, 2002.

DOI:10.1306/10170201045

AUTHORS

XIAORONG LUO ~ *Key Laboratory of Mineral Resources, Institute of Geology and Geophysics, Chinese Academy of Sciences, Beijing, 100029, China; xrxuluo@public.bta.net.cn*

Xiaorong Luo obtained his B.S. and M.S. degrees in geology from Northwestern University, China, where he taught petroleum geology for 5 years. He obtained his Ph.D. in geophysics from the University of Montpellier, France. His research interests of last 20 years have been in petroleum geology, currently focusing on numerical modeling, geopressuring, and hydrocarbon migration and accumulation.

WEILIANG DONG ~ *China Offshore Oil Nanhai West Company, Zhanjiang, Guangdong, 524057, China*

Weiliang Dong has a B.S. degree in geology from Southwestern Institute of Petroleum, China. He works on geological studies and management of hydrocarbon exploration for the China National Offshore Oil Company, with research interests on geological conditions of oil and gas accumulation and exploration of natural-gas plays. He conducted research on hydrocarbon systems in petroliferous basins and has over 20 years of exploration experience in Chinese offshore basins.

JIHAI YANG ~ *China Offshore Oil Nanhai West Company, Zhanjiang, Guangdong, 524057, China*

Jihai Yang obtained a B.S. degree in geology from Zhongshan University of China in 1985. He has worked on petroleum geology and natural-gas exploration, principally in Yinggehai and Qiongdongnan basins, for the China National Offshore Oil Company since 1985. His research interests are in hydrocarbon systems, especially hydrocarbon migration and accumulation in high-temperature and -pressure basins.

WAN YANG ~ *Department of Geology, Wichita State University, Wichita, Kansas, 67260; wan.yang@wichita.edu*

Wan Yang is an assistant professor researching in outcrop and subsurface sedimentology and stratigraphy of marine and nonmarine mixed-carbonate and siliciclastic rocks, paleoclimatology, and petroleum geology. He previously worked with Phillips Petroleum Company and the Bureau of Economic Geology, University of

Texas, on hydrocarbon exploration and exploitation. He holds a B.S. degree from Northwestern University, China, an M.S. degree from California State University, Fresno, and a Ph.D. from the University of Texas at Austin.

ACKNOWLEDGEMENTS

The authors benefited much from the discussions with G. Vasseur, J. Y. Wang, Z. S. Gong, Q. M. Zhang, S. T. Li, F. Hao, H. H. Chen, and X. N. Xie. We thank K. Magara, J. G. Gong, R. Erickson, and an anonymous reviewer for their suggestions. This study was supported partly by the Chinese National Major Fundamental Research Developing Project (G1999043310) and by the Chinese National Natural Science Foundation (49732005), both to X. R. Luo.

the permeable beds must be lower than or equal to those in the adjacent low-permeability formations. However, it has commonly been observed that pressures in reservoirs are higher than those in the adjacent low-permeability formations (e.g., Fertl, 1976; Grauls and Baleix, 1994). Some mechanisms have therefore been proposed to explain this phenomenon (Fertl, 1976; Barker, 1990; Osborne and Swarbrick, 1997; Luo et al., 2000).

Recent works indicate that quantitative methods are necessary to identify the relative importance of specific mechanisms in a given basin (Bethke, 1986; Shi and Wang, 1986; Luo and Vasseur, 1992; Osborne and Swarbrick, 1997). Basin models are commonly comprehensive, integrating and simulating individual geological and geophysical processes and phenomena (e.g., Ungerer et al., 1984; Lerche, 1990; Luo and Vasseur, 1992). A basin model must dynamically couple the principal geophysical fields, such as stress, geothermal, and hydraulic (Cao et al., 1989; Ungerer et al., 1990). Several studies showed that some overpressuring mechanisms are not effective under the general geological conditions of sedimentary basins (Bethke, 1986; Luo and Vasseur, 1992, 1996; Osborne and Swarbrick, 1997), and new mechanisms are needed to explain the observed overpressure phenomena in many basins (Luo, 1994; Luo et al., 2000).

The Yinggehai Basin in northwestern South China Sea is a Cenozoic rift-to-passive margin basin characterized by high temperature and overpressure (Gong et al., 1997; Hao et al., 1998, 2000). Several mechanisms have been proposed to qualitatively explain the characteristics of overpressuring in the basin: nonequilibrium compaction, aquathermal pressuring, smectite-to-illite transformation, and organic matter cracking-induced fluid generation (Liu, 1993; Zhang et al., 1996; Hao et al., 2000). However, they cannot fully explain the formation and distribution of overpressures in the basin.

This study attempts to quantitatively address the origin, formation, and distribution of overpressures in the Yinggehai Basin through numerical basin modeling. Consequently, a new overpressuring mechanism is proposed to explain the overpressure characteristics in the basin.

GEOLOGICAL BACKGROUND

The Yinggehai Basin is located on the continental shelf in the northwestern South China Sea (Figure 1A). It covers an area of about 500 $\times$ 50–60 km with the long axis oriented north-northwest to south-southeast (Zhang and Zhang, 1993). It developed from the Red River rift system in the early Cenozoic and has experienced three episodes of extension, accompanied with lithosphere stretching, mantle upwelling, and fast basin filling (Gong et al., 1997; He et al., 2000). The sedimentary fill is about 17 km thick at the basin center, where the crustal basement may be only 5 km thick (Gong et al., 1997).

The stress field in the basin was characterized by north-south stretching and east-west extension induced by the left-lateral strike

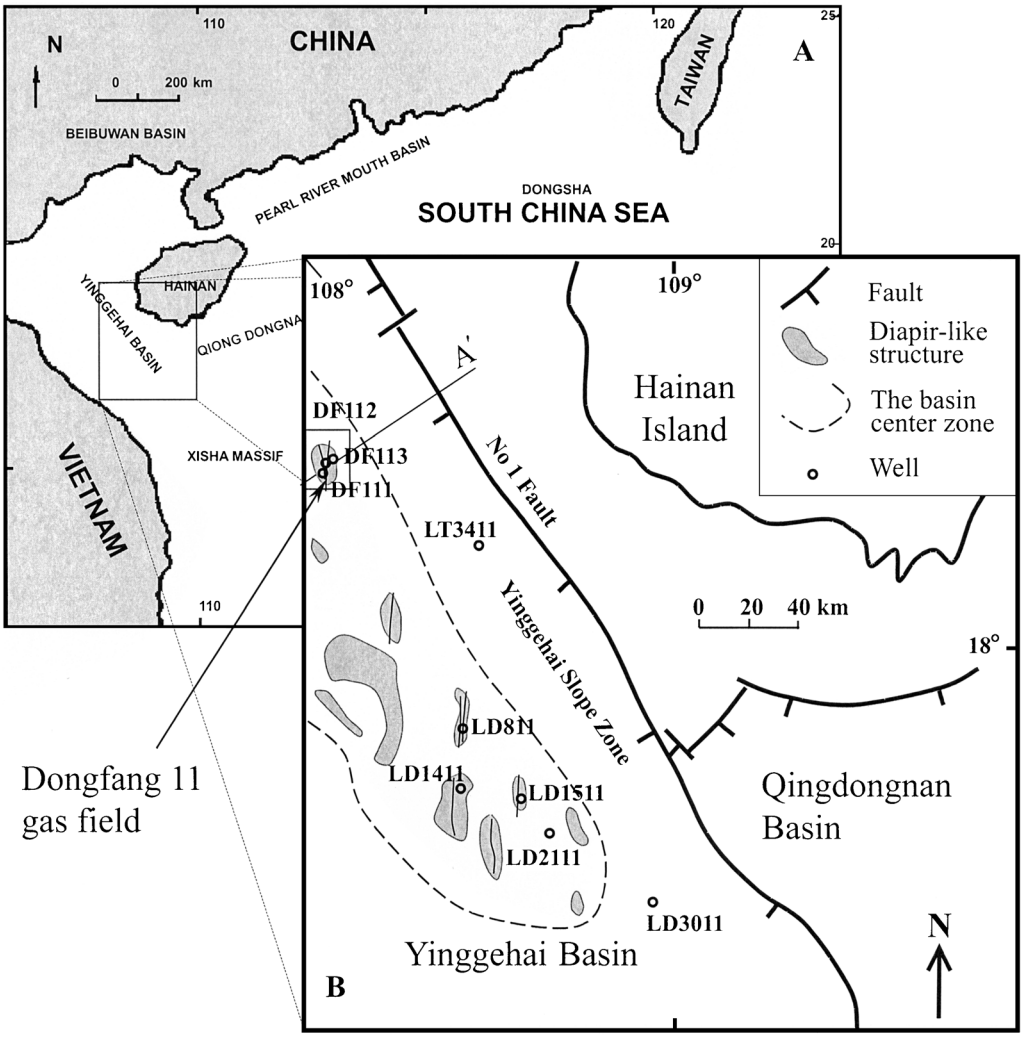

Figure 1. Diagram showing (A) the geographic location of the Yinggehai Basin, South China Sea and (B) the position of the section and the wells used in this article. Note the diapir-like structures in the center of the basin and the vertical episodically opening faults on these structures (modified from Chen et al., 1998; Hao et al., 2000).

basin-boundary faults at the early rift stage of basin development. The left-lateral motion changed to right-lateral during or after the Neogene, forming a stress field of east-west stretching and north-south extension in the basin (Gong et al., 1997; Wang, 2000). A series of en echelon, north-south–oriented folds formed at the basin center due to the left-lateral strike-slip faulting and were probably accentuated by the fast accumulation of a large amount of sediments (Figure 1B). After the Neogene, the east-west extensional stress associated with the right-lateral strike-slip faulting generated vertical fractures along the fold axes, extending for a great vertical distance. The folds and overlying sediments are called ''diapir-like structures'' in this study because the fracture zones are generally filled with gases and look like diapirs on seismic sections (Gong et al., 1997). It has been speculated that fluids at depth flowed upward along these fractures, resulting in geothermal and overpressure anomalies in shallow sediments on the diapir-like structures (Wang and Xie, 1998; Hao et al., 2000).

Fluvial and lacustrine sedimentation dominated in the basin during the rift stage, and marine siliciclastic and minor carbonate sedimentation took place during the postrift stage after the Eocene (Figure 2; Zhang and Zhang, 1993; Gong et al., 1997; Xie et al., 2001). The siliciclastic rocks are interbedded sandstone, siltstone, and mudstone. Thick and pure mudstones, which are favorable for generating and maintaining overpressure, are uncommon in the Neogene and Quaternary intervals, as indicated by well data (Gong et al., 1997; Chen et al., 1998).

OVERPRESSURE DISTRIBUTION IN THE BASIN

More than 40 wells have been drilled in the Yinggehai Basin. Most of them ended at a depth less than 1500 m.

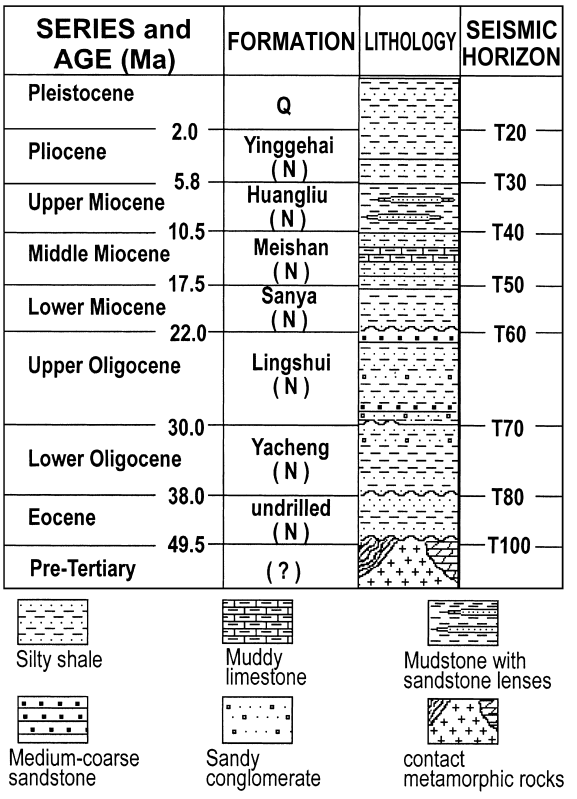

Figure 2. Chronology and lithostratigraphy in the Yinggehai Basin (modified from Chen et al., 1998).

The deep wells are generally located at the basin margin, where the pressures are mainly hydrostatic. In the basin center on the diapir-like structures, unpredicted overpressures were commonly encountered, forcing the drilling to end at shallow depths (1500–2000 m), such as in well LD1411 at 1560 m and in well LD2111 at 2300 m (Figure 1B; Gong et al., 1997).

Seismic interval velocity, logging data, and drillstem test (DST) or repeat formation tester (RFT) pressure measurements are analyzed to configure the current pressure distributions in the basin. The values estimated from the interval velocity and acoustic logs infer pore pressures in low-permeability formations, whereas DST or RFT measurements represent pressures in permeable formations. In some wells where the pressures were not measured, mud density data were used to estimate formation pressures because balanced drilling has been commonly practiced in the study area.

One-dimensional (1-D) compaction curves of 25 wells were generated using acoustic and density logs. Formation pressures were estimated from the curves using the balanced-depth method of Magara (1978) without considering the effect of aquathermal pressuring (Luo and Vasseur, 1992). The compaction trends vary in different formations because the high carbonate content in some layers and the presence of fractures and associated gases affect the compaction curves (Figure 3). A congruent method (Zhang et al., 2002) was used to identify and reduce these effects. In wells on the diapir-like structures, overpressures occur at shallow depth with some compaction anomalies (Figures 1, 4). However, the measured pressures are generally larger than those estimated from compaction curves.

Gong et al. (1997) estimated the pressure distribution in the Yinggehai Basin using several thousand kilometers of seismic velocity profiles of 180 seismic sections. They used a pressure coefficient (equal to estimated pressure divided by depth) of 1.2 to identify the top of the overpressured zone. It is deep at the basin margin, commonly about 4000 m, and becomes shallower toward the basin center, commonly at 1500–2800 m. Moreover, the magnitude of overpressuring at the basin center is much larger above the diapir-like structures than in the surrounding areas. The exact distribution and depth of overpressures vary irregularly among the diapir-like structures.

NUMERICAL MODEL

The characteristics of overpressures in the Yinggehai Basin raise two fundamental questions: How have the high overpressures been generated at such a shallow depth? Why are the pressures in permeable formations commonly higher than those in the low-permeability formations?

A numerical basin model, TPC-MOD (Luo and Vasseur, 1992; Luo, 1994), was used to identify the origin and mechanisms of overpressuring in the Yinggehai Basin. Modeling was carried out first using a 1-D stratigraphic column with simplified lithologies. The section represents the entire sedimentary rock column in the basin, where nonpenetrated intervals were interpreted from seismic data. Heat flow entering from the base of the section is a function of time following He et al. (2000). It is assumed that there is no fluid exchange at the base of the basin. The sediment-water interface is the upper boundary, where the water depth, temperature, and pressure are assumed constant in the course of basin development.

The effects of lateral lithologic variations on pressure and temperature are considered in modeling two-dimensional (2-D) sections. The effects are taken into account in modeling a fault opening that hydraulically

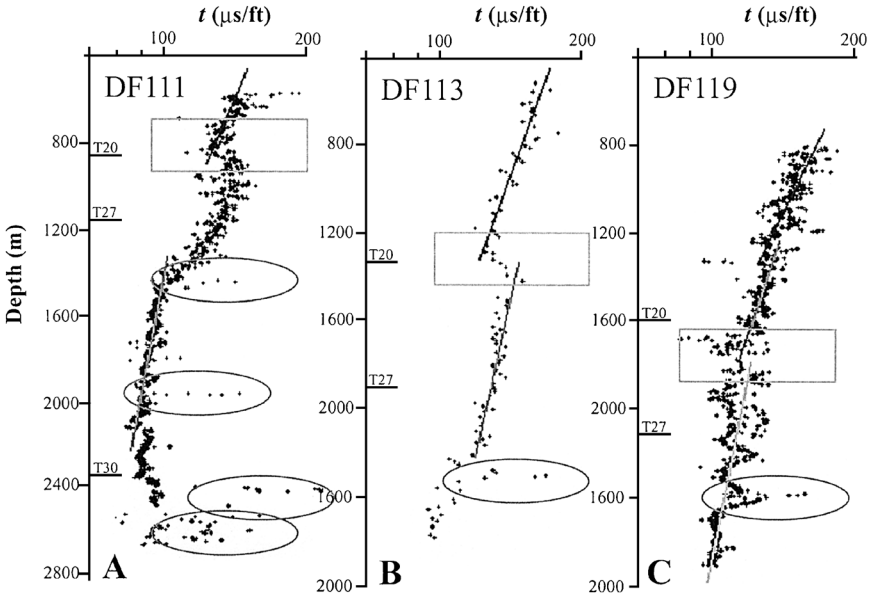

Figure 3. Compaction curves of three wells located in the basin center showing the effect of fractures and gas. The ellipses mark the formations containing gas-filled fractures. The rectangles mark the changes of compaction trends.

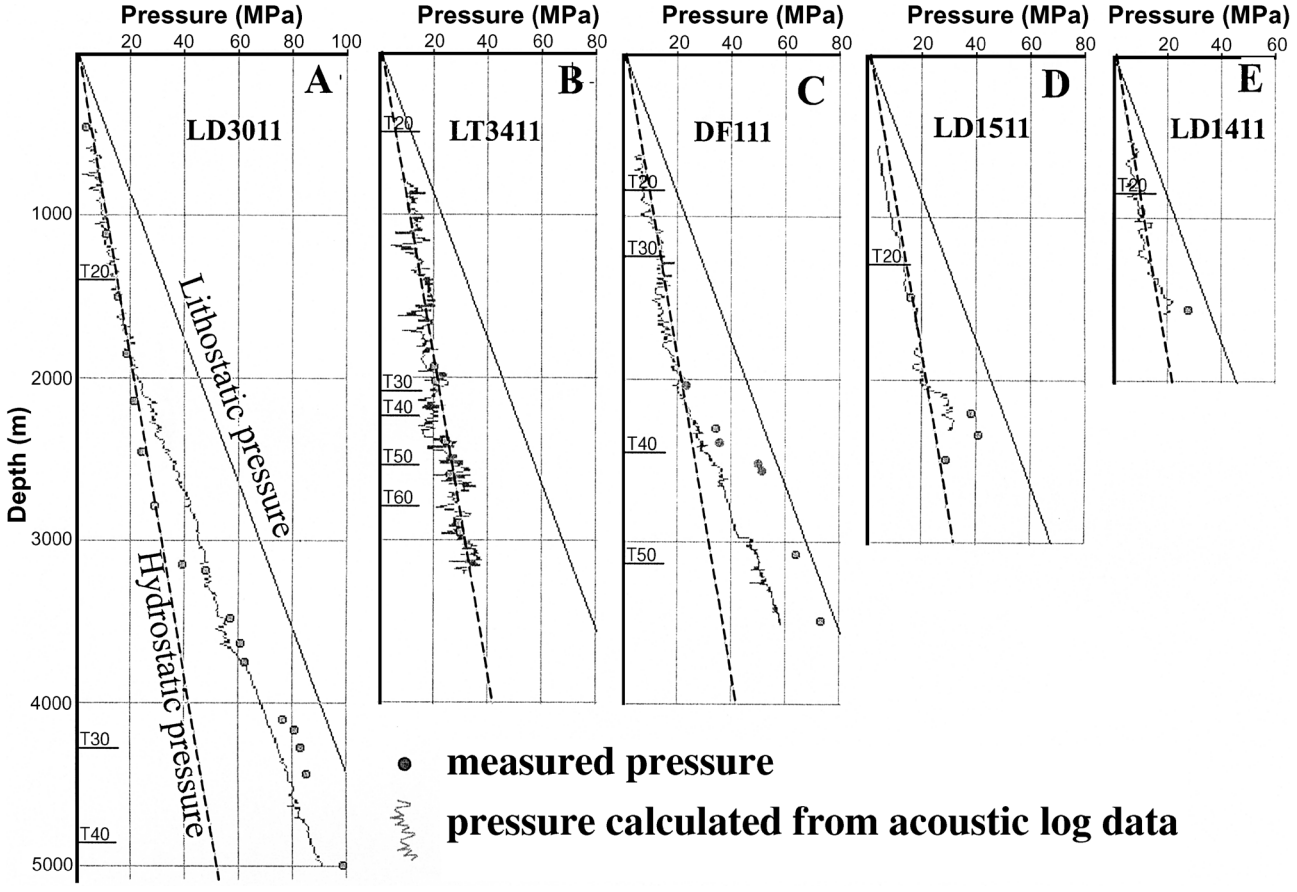

Figure 4. Representative pressure profiles in some wells in the Yinggehai Basin at the (A) southeastern part, (B) northeastern margin, and (C–E) center of the basin on the diapir-like structures (see Figure 1). Curves show the pressures calculated using the balanced-depth method from the compaction curves using acoustic log data. Solid dots represent the pressure measured by DST, RFT, or mud density. On panel (C), the DST data from other wells on the same structure (DF111) are marked on the pressure profile.

Table 1. Parameters Used in Numerical Modeling of This Study

Symbol	Parameters	Value	Unit
ρ	bulk density of pore fluid	1020	kg m^{-3}
ρ_s	bulk density of sediments' matrix	2720	kg m^{-3}
α	thermal expansibility of pore fluid	5.0×10^{-4}	$°C^{-1}$
β	compressibility of pore fluid	4.8×10^{-10}	Pa^{-1}
g	gravity	9.81	m s^{-2}

connects permeable formations separated by low-permeability formations. The boundary conditions in 2-D modeling are similar to those in 1-D modeling, except that the basal heat flow is a function of both time and location, which decreases from basin center to margins (He et al., 2000).

Model Parameters and Calibration

Model parameters that are commonly used in various basin models and in this study are listed on Table 1.

Acoustic log values of mudstones were used to calculate porosity to assess the behavior of mudstone compaction (Figure 5). The relationship between interval traveltime and porosity was derived from a modified Wyllie equation based on Wyllie et al. (1958):

$$\phi = C_p \frac{\Delta t - \Delta t_m}{\Delta t_f - \Delta t_m} \quad (1)$$

where ϕ is the total porosity of the rock; Δt, Δt_f, and Δt_m are the interval traveltimes of the rock as a whole, the pore fluid or mud in the borehole, and the matrix of the rock, respectively; and C_p is a correction coefficient to correct the porosity variation at shallow depths (Magara, 1978). The value of C_p ranges from a surface porosity ϕ_0 to 1.0 at a given depth z_s in this study. To characterize variation of C_p, an exponential relation was proposed in this work:

$$C_p = 1 - (1 - \phi_0) \cdot 10^{-\frac{z}{z_s}} \quad (2)$$

where z is the depth and z_s is the burial depth at which the fine-grained sediments are regarded as consolidated (i.e., $C_p = 1.0$ when $z \geq z_s$). Figure 5 shows the transformation from an acoustic data compaction profile to a porosity profile, and Table 2 lists the compaction coefficients obtained from some wells in the basin.

The compaction parameters of shales were then obtained from the compaction curves in each well. The average of initial porosity is about 0.60 and compaction coefficient is 4.5×10^{-4} m^{-1}. The porosity data of sandstones were synthesized from the porosity measurements published in Gong et al. (1997). The average initial porosity of sandstone is 0.40 and the compaction coefficient is 1.5×10^{-4} m^{-1}.

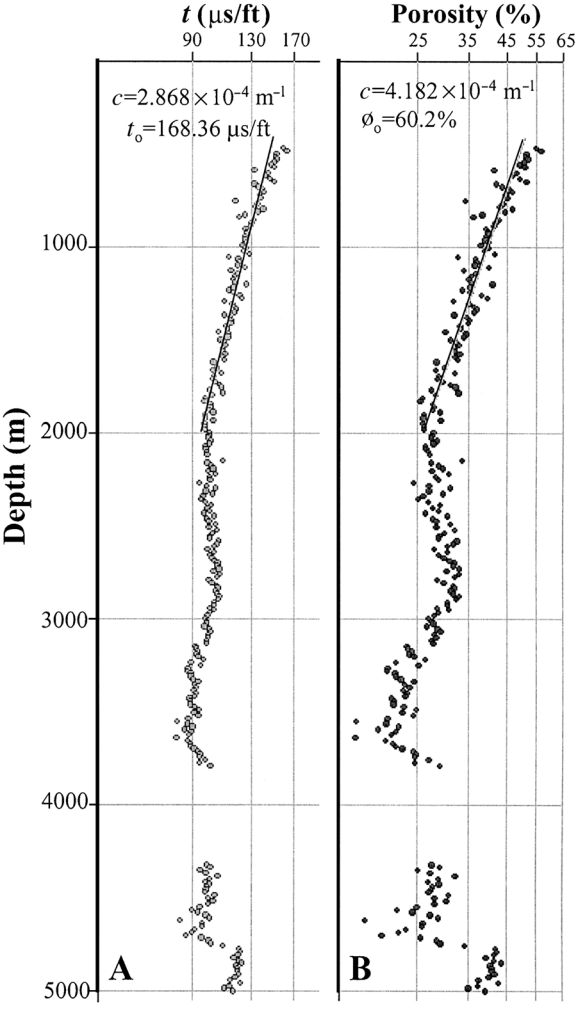

Figure 5. An example of the transformation from the compaction curve based on acoustic data to a porosity curve (well LD3011).

Table 2. Compaction Coefficients Obtained from Some Wells in the Yinggehai Basin

Well Name	Initial Porosity	Compaction Coefficient (m^{-1})
DF111	0.640	4.537×10^{-4}
LD1411	0.591	4.151×10^{-4}
LD1511	0.600	3.615×10^{-4}
LD3011	0.602	4.182×10^{-4}
LD811	0.613	4.049×10^{-4}
LT3411	0.620	4.380×10^{-4}

Six major types of sedimentary rocks and associated depositional environments in the basin were interpreted from well and seismic data by Gong et al. (1997): basinal lacustrine shale, shallow lacustrine shale and siltstone, basinal marine shale, shelfal marine shale and siltstone, littoral and marginal marine shale and siltstone, and sandstone and siltstone. Their compaction parameters were synthesized from the average values of mixtures of shale and sandstone (Table 3).

The compaction coefficients of shale-rich basin-slope deposits in the Yinggehai Basin range from 3.0×10^{-4} to 5.0×10^{-4} m^{-1} (Table 2). Compared with similar deposits in other basins (Magara, 1978; Bethke, 1986), the compaction coefficient of shale in the Yinggehai Basin is small, indicating poor alignment of clay minerals (Magara, 1978). Such slow compaction is not favorable for overpressuring because porosity and permeability reduction of the sediments with depth is slow (Magara, 1978; Luo et al., 1993).

Most of the parameters in the coupled relation among sediment compaction, evolution of basin geometry, and evolution of pore pressure required in the model can be explicitly derived from the actual data, except the coefficient that couples the porosity and permeability. A simplified porosity-permeability relation was used (Jacquin and Poulet, 1973; Luo and Vasseur, 1992):

$$k = \lambda\phi^n \tag{3}$$

where k is the permeability, n is the exponent that is about 5, and λ is an empirical constant related to lithology with a unit of 1 d (Jacquin and Poulet, 1973). One-dimensional modeling was done to calibrate the porosity-permeability constant λ (see next section).

Previous quantitative works (Bethke, 1986; Luo and Vasseur, 1992, 1996; Luo, 1994) suggest that the pressuring effects of aquathermal process and dehydration during smectite-illite transformation are minimal. Thus, these effects were not considered in the modeling. The organic content in well LD3011 is high compared with other parts of the basin. In this well, the average total organic carbon (TOC) is 1.95% in limestone and 1.95% in shale of the Ying-Huang Formation and 1.74% in limestone of the Meishan Formation; in other formations, the TOC values are commonly less than 0.6% (Gong et al., 1997). The organic matter cracking processes were modeled using TOC data and a kinetic model of Tissot and Espitalié (1975). The organic matter content in each lithology (Table 3) was synthesized from the previous works (Gong et al., 1997; Hao et al., 1998) and was assumed as null in sandstones. Gas production, the most important parameter in the model to identify the effect of organic matter cracking in overpressuring (Luo and Vasseur, 1996), increases significantly where sediments are buried deeper than 5000 m (Figure 6).

Overpressuring Modeling

A geological model was constructed from the deepest well LD3011 in the southeastern Yinggehai Basin (Figure 1), where faulting and hot-fluid activities have been limited

Table 3. Compaction Coefficients for Different Lithologies in the Yinggehai Basin*

Lithology	Initial Porosity	Compaction Coefficient (m^{-1})	OM Content (mg/mg)	OM Type
Littoral and marginal marine sandstone and siltstone	0.40	1.6×10^{-4}	0.00	–
Basinal lacustrine shale	0.63	5.2×10^{-4}	0.02	III
Shallow lacustrine shale and siltstone	0.48	3.2×10^{-4}	0.01	III
Basinal marine shale	0.53	4.8×10^{-4}	0.02	III
Shelfal marine shale and siltstone	0.48	3.2×10^{-4}	0.01	III
Littoral and marginal marine shale and siltstone	0.45	2.0×10^{-4}	0.006	III

*OM = organic material

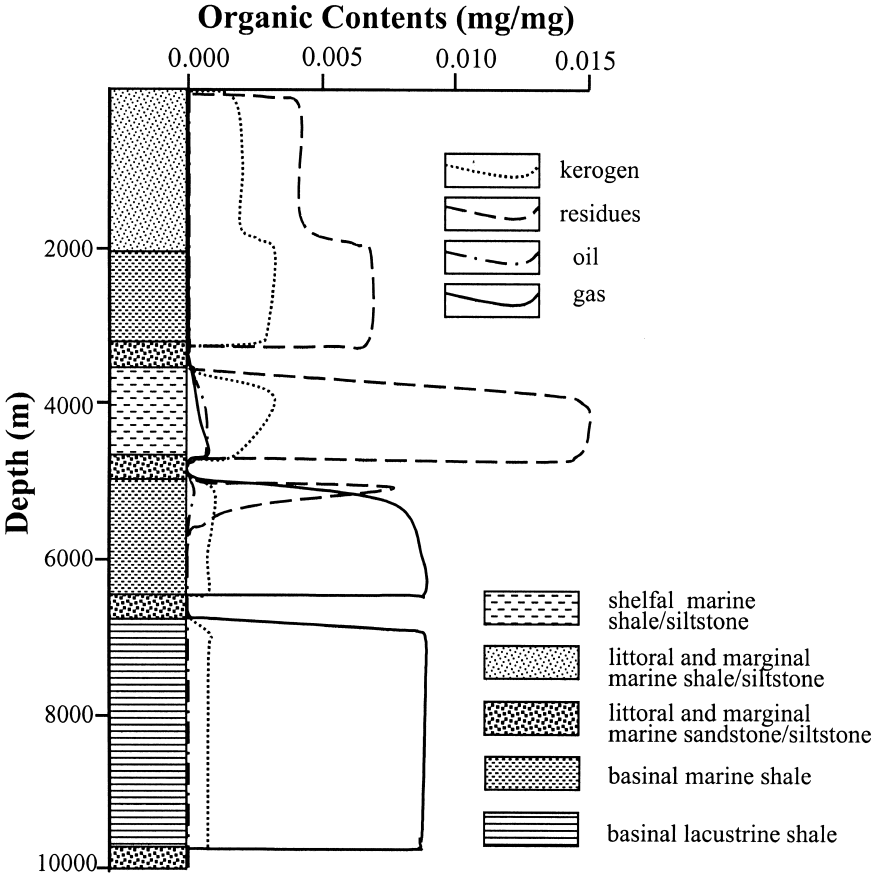

Figure 6. The distribution of variable organic matter contents in the current profile of well LD3011. The evolution and the percentages of organic cracking products are modeled using Tissot and Espitalié (1975).

(Zhang and Zhang, 1993; Xie et al., 2001). The present pressure distribution in the well was modeled using the aforementioned model (Figure 7). The pressure in low-permeable formations was calculated using the balanced-depth method (Fertl, 1976; Magara, 1978) from the compaction curve derived from acoustic data; the parameter λ was calibrated to approximate the pressure measures (Figure 7A). The drilling mud densities were transferred to equivalent pressures, approximating pore pressures in permeable formations.

The difference between the overpressure caused by disequilibrium compaction and that caused by both disequilibrium compaction and organic matter cracking is very small (Figure 7A), suggesting negligible pressuring effect of organic matter cracking in this case.

In addition, where the modeled pressures fit well with those estimated from disequilibrium compaction, the permeability constant λ was calibrated as 8.0×10^{-5} d for Pliocene and Quaternary marine shales, 2.0×10^{-5} d for Miocene marine shales, 1.0×10^{-5} d for Oligocene lacustrine shales, and 1.0×10^{-2} d for Oligocene siltstones.

The parameters derived from 1-D modeling of well LD3011 were used to model the pressure distributions in wells on the diapir-like structures. The results suggest that neither disequilibrium compaction nor organic matter cracking can cause the high pressures observed in the shallow permeable formations on these structures.

Open-Fault Connection Model

The results of 1-D modeling suggest that other overpressuring mechanisms, rather than disequilibrium compaction and organic matter cracking, may have been a significant factor in generating and maintaining high overpressures in the permeable formations on the diapir-like structures. A model of an open fault connecting overpressure compartments is proposed to explain the origin of these overpressures.

A 2-D geological model was established based on geological interpretations of wells on the diapir-like structures and nearby seismic sections (Figure 8). The fault-opening process was realized in a 2-D numerical model based on the geological model to quantitatively assess the performance of the open-fault connection model. In the numerical model, the fault is represented by a sediment column. When the fault opens, the permeability of sediment in the column increases several orders. As a result, a favorable hydraulic condition

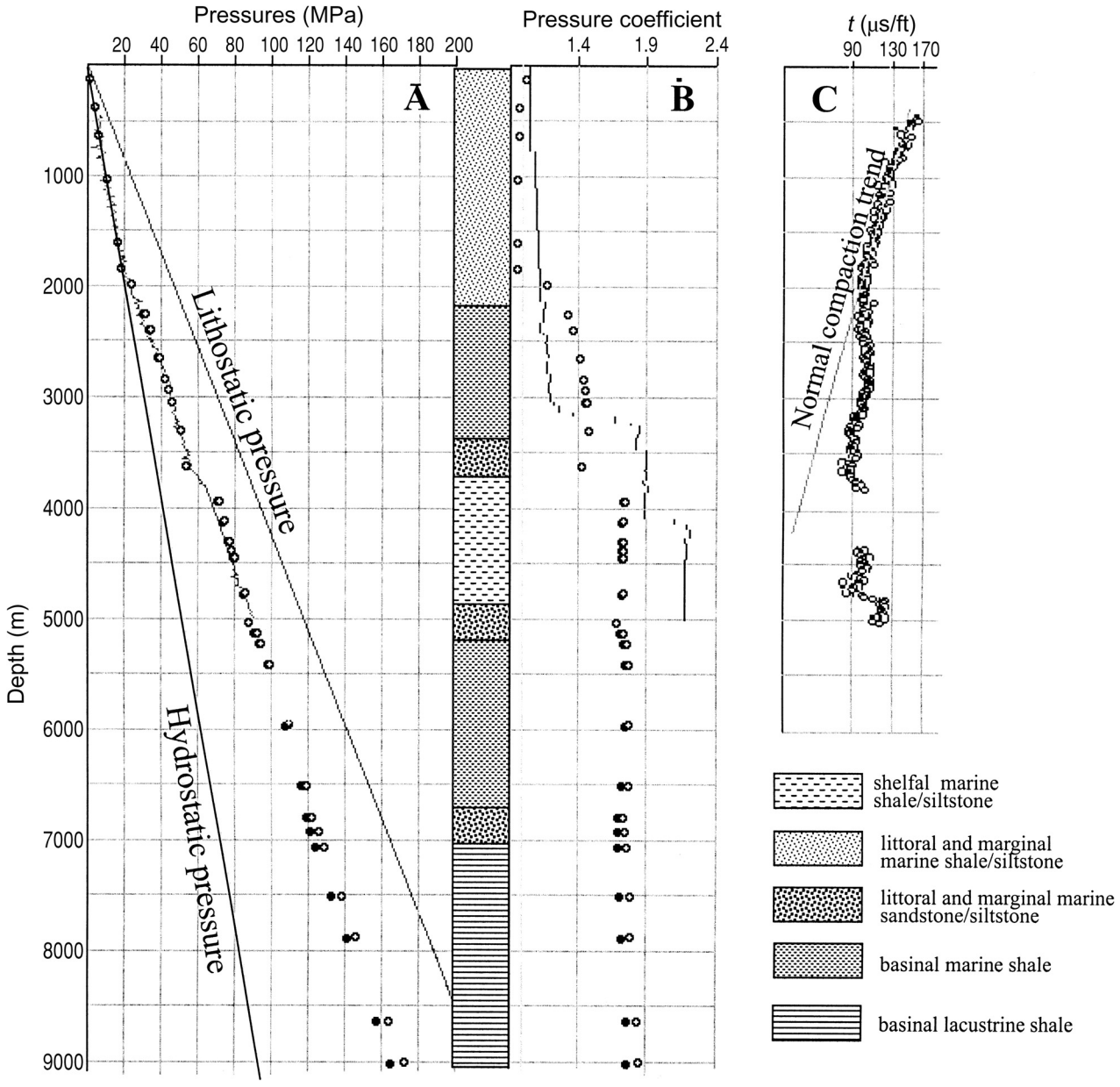

Figure 7. Model results of well LD3011. (A) Modeled pressures with consideration of disequilibrium compaction (solid dots) and with both disequilibrium compaction and organic matter cracking (open circles). The fine curve is the fit to the pressure distribution using a select λ value. The lithology column was constructed using well and seismic data. (B) Corresponding pressure coefficients. The curve represents the equivalent mud pressure coefficient. (C) Compaction curve constructed using acoustic log data of mudstones (open circles).

is established in the column so that both fluid and fluid pressures are readjusted among the connected reservoirs.

Figure 9 shows the 1-D model results on a section constructed using well LD1411 and nearby seismic section on a diapir-like structure in the basin center (Figure 1). A pressure value of 27 MPa was measured in the reservoir at 1560 m (Figure 9B), which is, in fact, close to the fracturing pressure at this depth, where the lithostatic pressure is only 32 MPa because the overlying sediments have not been well compacted. In the model, a fault near the well has opened episodically during 0.46–0.0 Ma and served as a conduit to channel the deep pressure into the shallow reservoir at 1570 m. The vertical distribution of porosity and pressures in both permeable and low-permeability formations were used as the calibration data (Figure 9C). The fault was assumed as a parallel plate filled with sediments of a thickness of 10 m. Its transmissibility is assumed as 10^{-15} m^2 when it opens and as 10^{-24} m^2 when it closes. Following Snow (1969) among others, the permeability

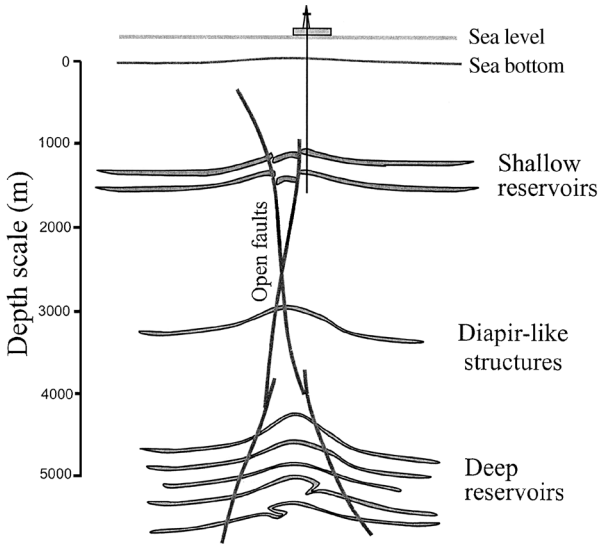

Figure 8. A geological model illustrating that the reservoirs at different depths are hydraulically connected by subvertical open faults. This connection causes readjustment of fluid and pressure between deep, high-pressure reservoirs and shallow, low-pressure reservoirs.

value of the fault at opening state corresponds with a fault with an opening width of 2.3×10^{-5} m.

The model results show that fault-opening and connection processes can easily produce a high pressure in shallow permeable formation (Figure 9A, B). The coupled processes among episodic fault opening, pressure readjustment, and continuous deposition generated pressure and porosity profiles that closely match those observed in well LD1411. Model results provided insight into the dynamic pressure evolution within the upper 5000 m during an episode of fault opening and closing (Figure 10). Similar success was also achieved for other wells on the diapir-like structures in the basin center.

Two-Dimensional Numerical Modeling

With the understanding of the overpressure distribution and generating mechanisms through 1-D modeling, the overpressure evolution on a 2-D cross section was modeled using the 2-D numerical model of Luo (1994) (see

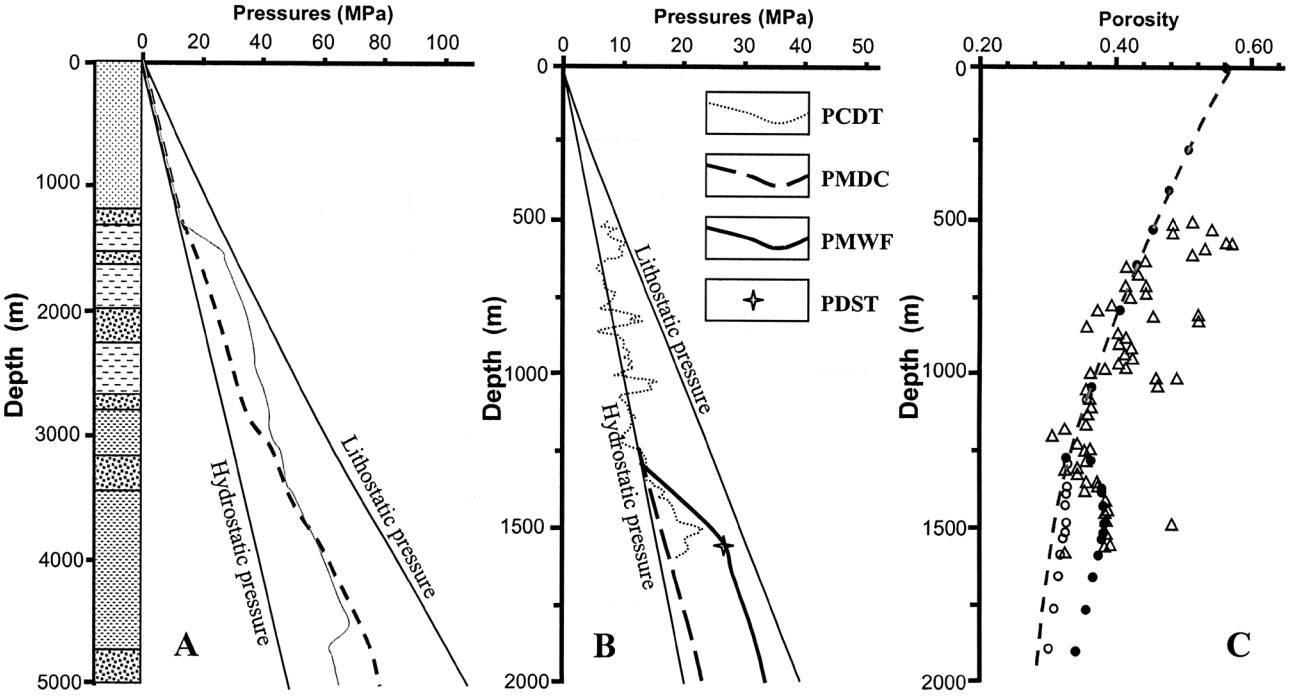

Figure 9. Model results using the open-fault allogenic mechanism for well LD1411 located on a diapir-like structure in the basin center. (A) Modeled pressures with consideration of fault opening (solid line) and without consideration of fault opening (dashed line). (B) A close-up of modeled pressure distribution in the shallow interval. PCDT = pressure calculated from acoustic log data; PMDC = pressure modeled without fault opening; PMWF = pressure modeled with fault opening; PDST = DST pressure measurement. Notice the good match between PMWF and PDST. (C) Undercompaction caused by allogenic pressuring. The thick dashed curve represents the normal compaction trend, the triangles represent the porosity values calculated from acoustic log data, the solid dots represent the porosity modeled with episodic fault opening, and the open circles represent the porosity modeled without fault opening. Notice the good match between the acoustic porosity points and those modeled with episodic fault opening.

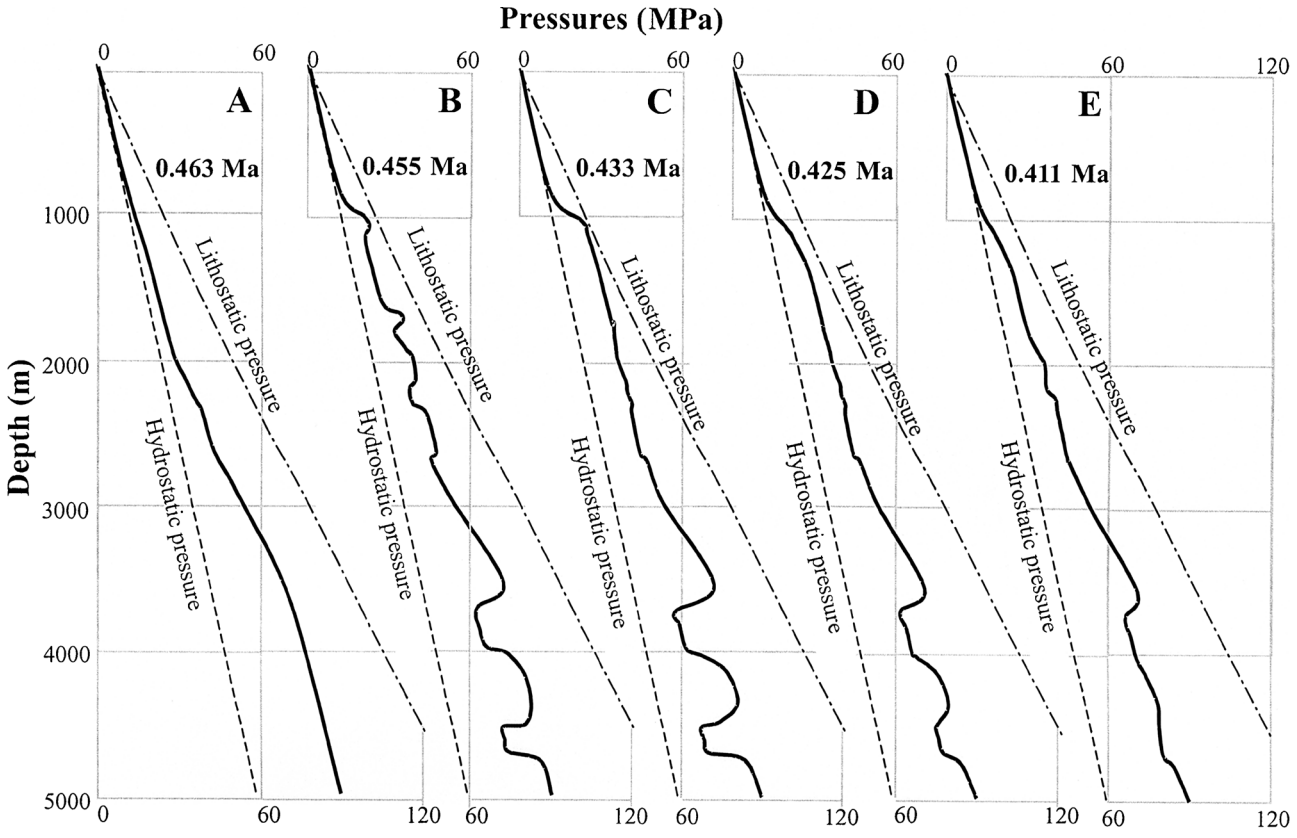

Figure 10. Model results showing the dynamic changes of formation pressure during an episode of fault opening and closing for well LD1411. Panels (A–E) show five stages of pressure distribution when the fault is closed, just before opening, just after opening, opening, and just closed and before next opening.

also Luo and Vasseur, 1992, 1996). The 2-D geological model was constructed from the geological interpretation of a regional seismic section (Figure 1). Six types of lithologies were interpreted from well and seismic data (Figure 11).

In the 2-D numerical model, the lateral stratigraphic boundaries were defined at the positions where the basin topography and formation thickness change slightly. The boundary conditions were therefore simplified: there is no heat flow or fluid movement across the lateral boundaries, the heat flow varied laterally at the bottom boundary (He et al., 2000), and there is no fluid flowing through the bottom boundary. Both temperature and pressure were kept constant at sea floor during basin evolution.

A vertical fault near well LD111 on the diapir-like structure (Figure 1) was assumed to have opened episodically since 0.8 Ma. The fault-opening interval is 0.03 m.y. and the duration of an opening period is 0.3 m.y. (thus, the fault is closed at present). The fault was also assumed as a parallel plate filled with sediments of a thickness of 10 m. Its transmissibility is assumed as 10^{-15} m^2 when it opens and as 10^{-24} m^2 when it closes. The pressures calculated from acoustic log data and from direct measurements were used to calibrate the model results. The other model parameters are listed in Tables 1 and 2.

Figure 12 shows the modeled distribution and evolution of excess pressure, which is equal to the difference between the modeled pressure and the hydrostatic pressure, in the selected section. During most of the period of basin development, basin topography and lithology mainly controlled the spatial variation of excess pressure. It was zero at the sediment surface and it increased slightly within the interval from 1800 to 3000 m (Figure 12A–C). The excess pressure increased significantly in formations deeper than 3000 m. However, the current pressure distribution in the interval shallower than 3000 m is largely controlled by the fault opening (Figure 12D).

The effect of fault opening on pressure evolution and distribution is further illustrated in Figure 13, where the vertical coordinate is enlarged and excess pressures are illustrated by contours. Before fault opening, the excess

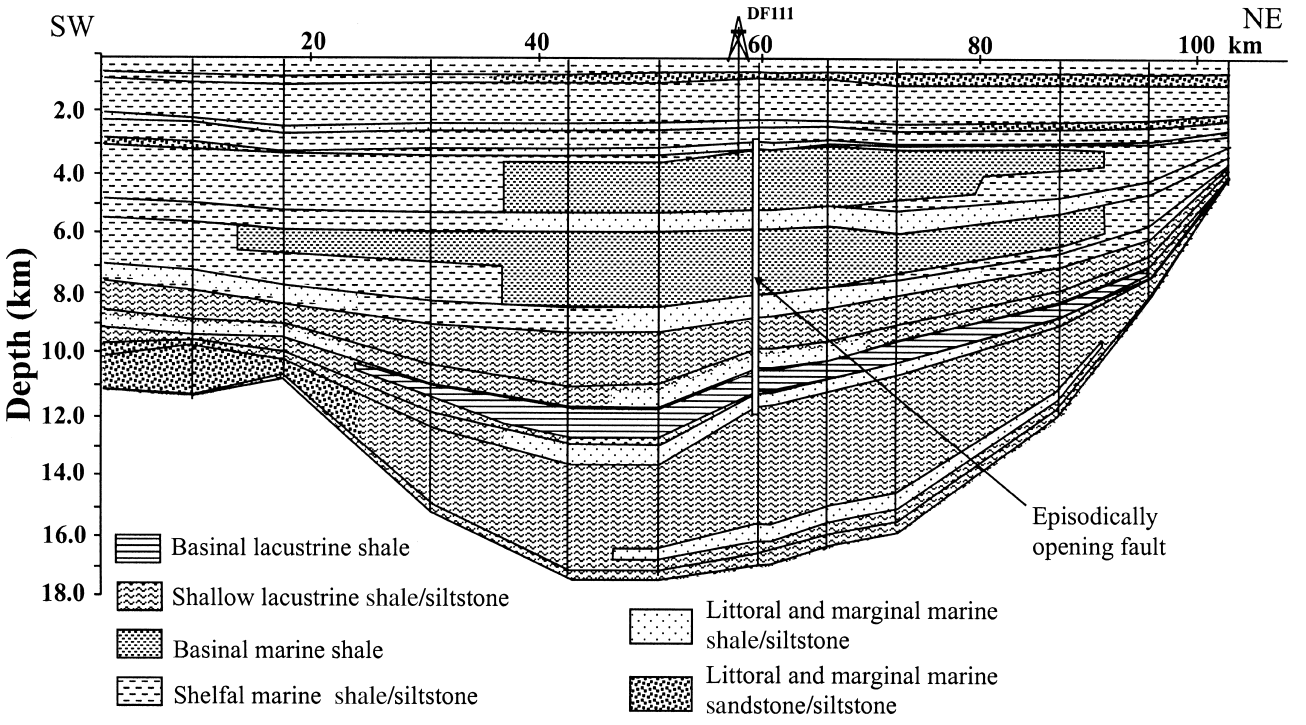

Figure 11. A regional northeast-southwest cross section of the Yinggehai Basin (see Figure 1 for location) that was used as the 2-D geological model in the numerical modeling. The vertical lines represent pseudowells constructed from seismic data. A fault, located at the 60-km mark and with a white rectangle representing its position and vertical extent of opening, has opened episodically since 0.8 Ma.

pressure was generated relatively uniform within the low-permeability formations (Figure 13A). When a fault opened at the basin center, the pressures in the permeable formations connected by the fault were readjusted completely so that the excess pressures are similar among them (Figure 13B). As a result, the top of the overpressure zone rose to formations shallower than 2000 m (comparing Figure 13A and B). Pressure increased not only in permeable formations, but also in the adjacent low-permeability formations. The pressure distribution in low-permeability formations after fault opening, however, is, overall, similar to that before the fault opening; the readjustment occurred only within a narrow interval along the interface with permeable formations or the opening fault. Along the narrow interface, the excess pressure contours are dense and parallel to the interface.

DISCUSSION

Allogenic Overpressuring Mechanism

The overpressure in the shallow formations in the Yinggehai Basin is allogenic because the source of pressure lies far below and is separated from the shallow formations. Thus, the presence of high overpressures in deep formations is a prerequisite for this mechanism.

When reservoirs of very different excess pressures are hydraulically connected, the pressure in different reservoirs readjusts quickly, but not within the intervening seals, because the hydraulic reaction of low-permeability seals is very slow relative to a short period of fault opening (Luo, 1999). The hydraulic readjustment and the different rates of readjustment between permeable and low-permeability formations generate a very heterogeneous pressure distribution in the shallow intervals. The pressure in reservoirs is much greater than the adjacent seals, and the pressure within the reservoirs increases with depth along the hydrostatic gradient (Figures 9, 13).

This study suggests that in the shallow interval, pressure increase occurred earlier in reservoirs than in seals, as proposed by Swarbrick and Osborne (1996). As a result, the pressure in reservoirs is higher than that in the intervening seals. The high pressures in the reservoirs are then transmitted to the neighboring seals diffusively (Deming, 1994; He and Corrigan, 1995). With time, the pressure increases in the seals and decreases in reservoirs.

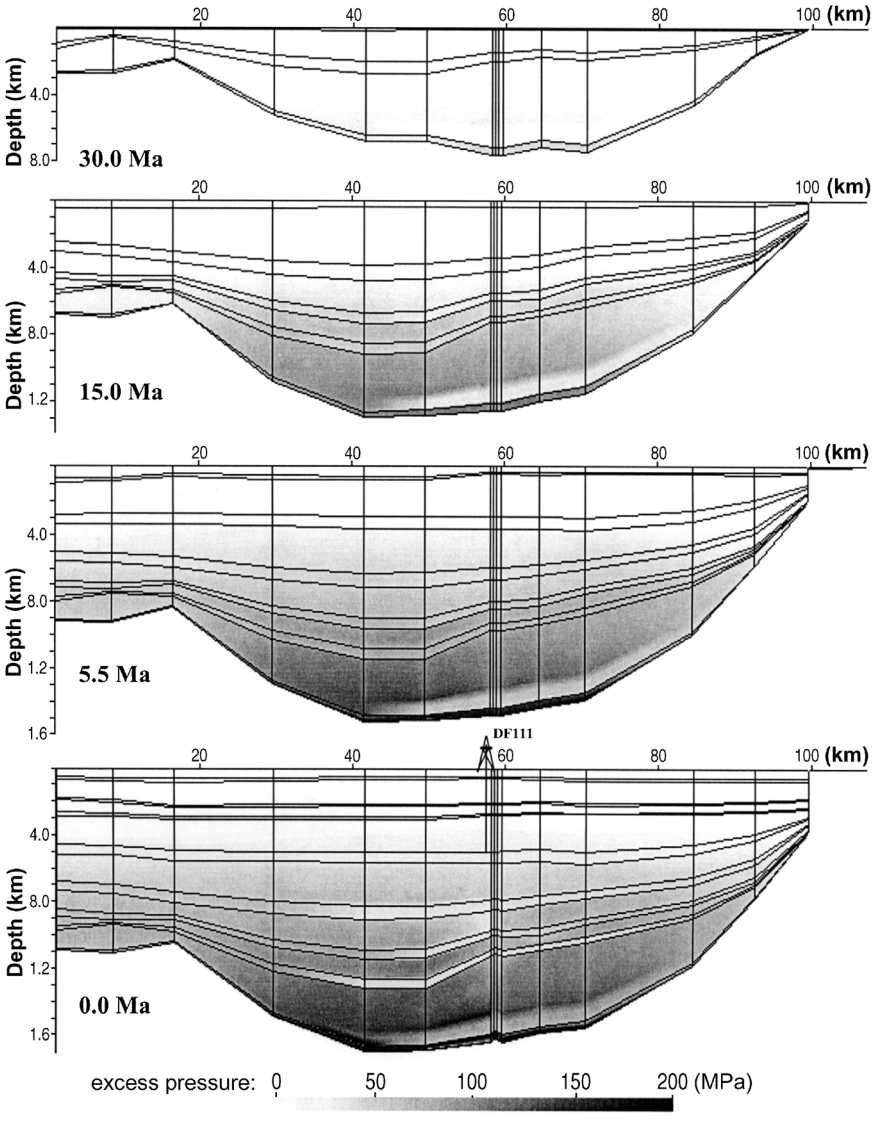

Figure 12. Two-dimensional numerical model results showing the distribution of excess pressure at 30, 15, 5.5, and 0 Ma.

Pressuring Conditions

Certain geological conditions are necessary to generate and maintain overpressures in shallow reservoirs because the hydraulic conditions in shallow intervals are not, in general, favorable for overpressuring. This is true for shallow formations in the center of the Yinggehai Basin where sediments have been compacted slowly and thick pure shales are lacking. In addition, when a fault opens, the entire system, including all the connected reservoirs and other faults, must be sealed.

The duration of overpressures in the shallow reservoirs is determined mainly by the sealing capacity of the shallowest seal (Deming, 1994; He and Corrigan, 1995). Luo and Vasseur (1997) analyzed pressure diffusion in a seal-reservoir model where a seal lies upon an overpressured reservoir bed, assuming that the pressure in the reservoir can only dissipate diffusively through the seal and that the pressure in a reservoir overlying the seal is hydrostatic. The diffusion time when the pressure in the reservoir is totally dissipated is (Luo and Vasseur, 1997)

$$\tau = \frac{S'l'^2}{3K'}\left(1 + \frac{3Sl}{S'l'}\right) \tag{4}$$

where l and l' are the thicknesses of the reservoir and the seal, respectively; S and S' are the specific storages of reservoir and seal, respectively; and K' is the hydraulic conductivity of the seal.

In a system of reservoirs connected by open faults, if the total thickness of individual reservoirs is regarded as the reservoir thickness (l) in equation 4, the shallowest low-permeability formation in this study would

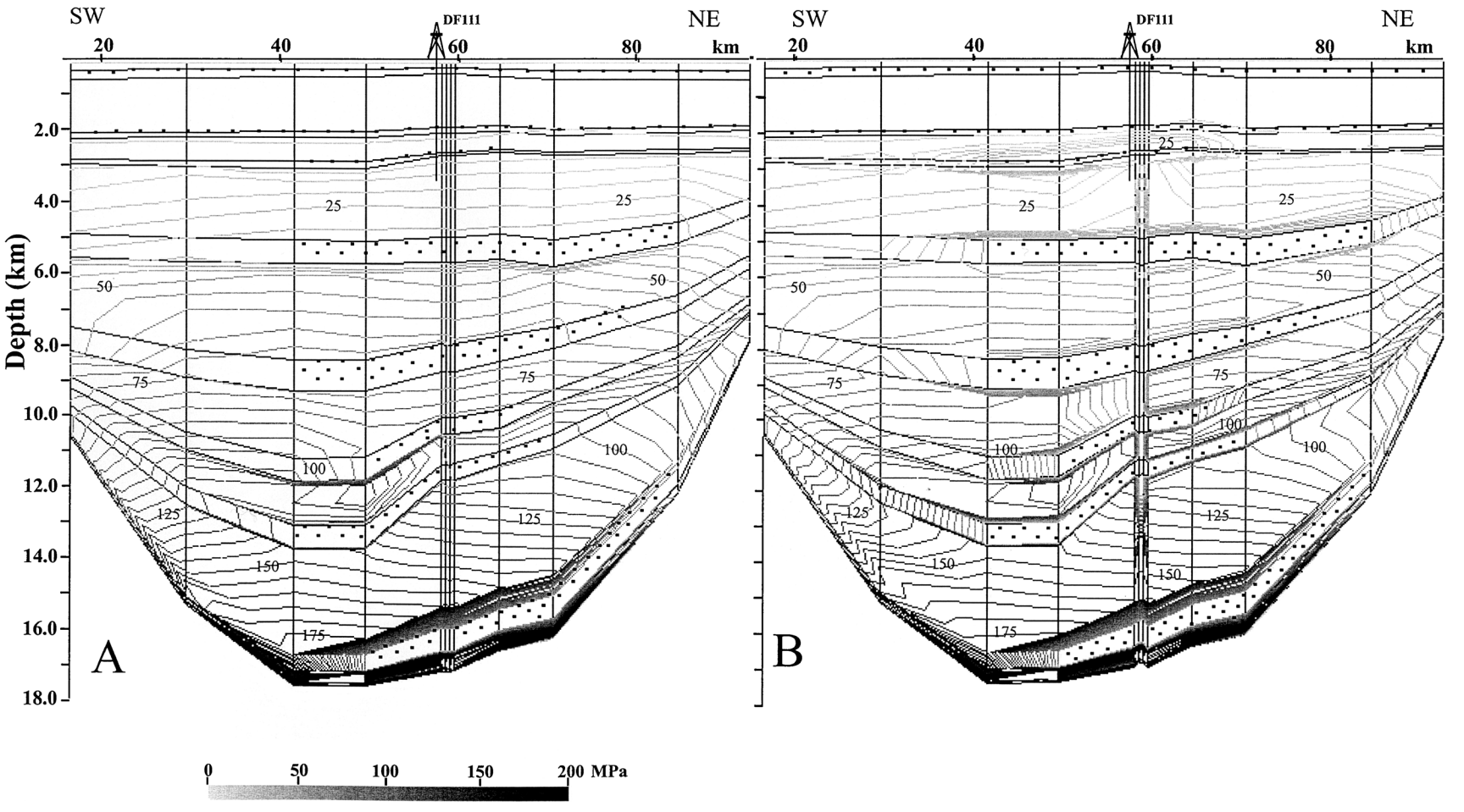

Figure 13. Distribution of excess pressure just before (A) and after (B) the first episode of fault opening at 0.8 Ma showing the significant readjustment of formation pressure after fault opening. The formations with a dotted pattern are the main permeable sandstones.

be equal to the seal in the previous model. Therefore, the overpressure lasting time of the system depends mainly on the thickness, compaction coefficient, and permeability of the low-permeability formation. The total thickness of the reservoirs connected by the open fault and the compacting effect of the reservoir will influence the diffusion process. In equation 4, the first term represents the sealing capacity of the shallowest low-permeability formation, and the second term represents the amount of fluid transmitted from reservoirs during fault opening.

It has been documented that some basins have low-permeability seals to maintain temporarily the overpressures in shallow reservoirs, which have a deep pressure source (Grauls and Baleix, 1994).

A large quantity of gases in the shallow reservoirs and surrounding seals will change the rock permeability by changing the fluids in the system from single phase to two phases (Surdam et al., 1994). The Yinggehai Basin has abundant methane gas in the shallow formations on diapir-like structures, which was mainly generated in source rocks buried below 4000 m (Gong et al., 1997; Xie et al., 2001).

Episodic fault opening facilitates fluid migration between otherwise isolated reservoirs. When a fault opens, pressure increases in the shallow reservoirs and decreases in the deep reservoirs. Decreased pressure at depth tends to cause the opening fault to close, as the effective stress state has been reduced (Jaeger and Cook, 1979; Nunn, 1996). However, the pressure in low-permeability formations surrounding the deep reservoirs does not decrease significantly because of their low-fluid diffusion rate during the fault opening (Luo, 1999). As a result, fluid at depth moves continuously from the low-permeability formations to the adjacent reservoirs during and after the fault opening. During the fault-closing period, the continual fluid transmission at depth causes gradual pressure increase in the deep reservoirs to eventually cause the next fault opening (Roberts and Nunn, 1995). The deep-buried low-permeability formations commonly contain enough pore fluid to maintain the episodic fault opening and, thus, large excess pressures in the shallow reservoirs.

Allogenic Overpressuring and Undercompaction

In the Yinggehai Basin, the undercompacted, low-permeability formations overlying the open-fault system (Figure 9) indicate that the high overpressures in the shallow reservoirs have been maintained for a long period.

The overpressures in the shallow seals have been generated mainly by pressure diffusion from neighboring reservoirs, and their porosity would not increase to cause undercompaction because compaction is an irreversible process (Magara, 1978; Charlez, 1991). However, if the next fault opening occurs before complete dissipation of the excess pressure in the shallow reservoirs while deposition continues at surface, undercompaction in the seals overlying the shallow reservoirs occurs. This is the case in the Yinggehai Basin. Besides episodic fault opening, sedimentation rate has been high, 300–600 m/m.y. on average since the Pliocene (Gong et al., 1997; He et al., 2000).

Pressure Evolution and Distribution after Fault Opening

The episodic fault opening and closing complicate the pressure distribution and evolution in the basin. The model results for well LD1411 illustrate the pressure evolution (Figure 10). Before fault opening, pressures in formations shallower than 2600 m are very small and nearly hydrostatic (Figure 10A). When the fault opens, the pressure increases in the reservoirs in the interval from 1300 m (1580 m at present) to 2700 m and decreases in the reservoirs within the intervals of 4500–4800 and 5600–5800 m (Figure 10B). However, the pressures in the seals separating the shallow reservoirs increase slowly due to slow pressure diffusion from the reservoirs. After a period of fault opening, the pressures in the shallow interval become nearly uniform and excess pressures are nearly the same among the reservoirs (Figure 10C). When the fault closes, the deep fluid source was cut off and the pressure decreases gradually in shallow reservoirs and increases in deep ones (Figure 10D). After a period of fault closure, the pressures in the shallow formations decease further whereas the pressures in the deep reservoirs gradually increase due to fluid transmission from neighboring seals (Figure 10E). The distribution of measured pressures in the formations on the DF111 structure may indicate pressure regeneration in the permeable formations after fault closure (Figure 4C).

When the fault reopens, the pressure in the deep interval decreases but is still much larger than the hydrostatic pressure. This results in complex pressure changes and pressure distribution, such as the high pressures in the reservoir at 1580 m and the undercompacted seal from 1450 to 1580 m in well LD1411 (Figure 9).

On a 2-D section (Figure 12), the excess pressures developed in accordance with the basin filling before 0.8 Ma, as deposition has occurred nearly continuously

since 40 Ma, although the deposition rate varied in space and time (Gong et al., 1997; He et al., 2000). However, when a fault opened on a diapir-like structure, the pressure distribution evolved to a very heterogeneous state (Figure 12D). The lateral extent of the influence by the fault opening depends on the hydraulic connectivity of the reservoirs.

The distribution of excess pressure without faults in the section was controlled mainly by the basin geometry. The lithologic variations caused minor anomalies (Figure 13A). However, when a fault opens at the middle interval, but not through the entire section, the distribution of excess pressure changes drastically. The excess pressures in all reservoirs connected by the open fault become the same and a large excess pressure appears in the reservoir buried at 2500 m (Figure 13B). Within the seals between connected reservoirs, the contours become parallel to the interfaces and along the fault (Figure 13B) indicating steep excess pressure gradients. The pressure distribution suggests that the pressure diffusion patterns are very different between reservoirs (permeable) and seals (low permeability) (Luo, 1999).

CONCLUSIONS

Numerical modeling of the overpressure distribution and evolution in the Yinggehai Basin shows that overpressuring generated by disequilibrium compaction is insignificant at a depth less than 2400 m. Organic matter cracking is a minor factor in overpressuring even within the zone where organic cracking is the most active. This is because the organic matter content is low in this basin and the permeability of shallow-buried Neogene and Quaternary formations is not low enough.

An allogenic pressuring mechanism is proposed to explain the overpressure distribution in the Yinggehai Basin. When two reservoirs, originally with quite different excess pressures, are connected hydraulically by an open fault, pressure readjusts between them quickly. As a result, relatively high abnormal pressure occurs in the shallow reservoirs that originally had relatively low excess pressure.

Episodic fracturing and faulting are the major causes of overpressure in shallow intervals. As sediment deposition continued when shallow reservoirs were overpressured, the pressure diffusion in the adjacent low-permeability formations may have resulted in some undercompaction. However, pressure in the shallow, undercompacted, low-permeability formations is much lower than that measured in the neighboring reservoirs.

REFERENCES CITED

Barker, C., 1990, Calculated volume and pressure changes during the thermal cracking of oil to gas in reservoirs: AAPG Bulletin, v. 74, p. 1254–1261.

Bethke, C. M., 1986, Inverse hydrologic analysis of the distribution and origin of Gulf Coast-type geopressured zones: Journal of Geophysical Research, v. 91, p. 6535–6545.

Cao, S., I. Lerche, and W. G. Lyon, 1989, One-dimensional modelling of episodic fracturing: a sensitivity study: Terra Nova, v. 1, p. 177–181.

Charlez, A., 1991, Rock mechanics, volume 1, theoretical fundamentals: Paris, Éditions Technip, 335 p.

Chen, H. H., S. T. Li, Y. C. Sun, and Q. M. Zhang, 1998, Two petroleum systems charge the YA13-1 gas field in Yinggehai and Qiongdongnan basins, South China Sea: AAPG Bulletin, v. 82, p. 757–772.

Deming, D., 1994, Factors necessary to define a pressure seal: AAPG Bulletin, v. 78, p. 1005–1009.

Fertl, W. H., 1976, Abnormal formation pressure, implication to exploration, drilling, and production of oil and gas reservoirs: Amsterdam, Elsevier, 382 p.

Gong, Z. S., S. T. Li, T. J. Xie, Q. M. Zhang, J. M. Yang, Y. C. Sun, and L. H. Liu, 1997, Continental margin basin analysis and hydrocarbon accumulation of the Northern South China Sea (in Chinese): Beijing, Science Press, 510 p.

Grauls, D. J., and J. M. Baleix, 1994, Role of overpressures and in situ stresses in fault-controlled hydrocarbon migration: a case study: Marine and Petroleum Geology, v. 11, p. 734–742.

Hao, F., Y. C. Sun, S. T. Li, and Q. M., Zhang, 1998, Overpressure retardation of organic-matter maturation and hydrocarbon generation: a case study from the Yinggehai and Qiongdongnan basins, offshore South China Sea: AAPG Bulletin, v. 79, p. 551–562.

Hao, F., S. T. Li, Z. S. Gong, and J. M. Yang, 2000, Thermal regime, interreservoir compositional heterogeneities, and reservoir-filling history of the Dongfang gas field, Yinggehai Basin, South China Sea: evidence for episodic fluid injections in overpressured basins: AAPG Bulletin, v. 84, p. 607–626.

He, Z. Y., and J. Corrigan, 1995, Factors necessary to define a pressure seal: discussion: AAPG Bulletin, v. 79, p. 1075–1078.

He, L. J., L. P. Xiong, J. Y. Wang, J. H. Yang, and W. L. Dong, 2000, Modeling on the structure-geothermal evolution in the Yinggehai Basin (in Chinese): Science in China (Series D), v. 30, p. 415–419.

Jacquin, C., and M. Poulet, 1973, Essai de restitution des conditions hydrodynamiques régnant dans un bassins sédimentaire au cours de son évolution: Revue de l'Institut Français du Pétrole, v. 28, p. 269–297.

Jaeger, J. C., and N. G. Cook, 1979, Fundamentals of rock mechanics: London, Chapman and Hall, 593 p.

Lerche, I., 1990, Basin analysis, quantitative methods, v. 1: San Diego, California, Academic Press, 562 p.

Liu, F. N., 1993, Identify potential sites of gas accumulation in overpressure formation in Qiongdongnan Basin of South China Sea: AAPG Bulletin, v. 77, p. 888–895.

Luo, X. R., 1994, Modélisation des surpressions dans les bassins sédimentaire et des phénomènes associes: Ph.D. thesis, Université Montpellier II, France, 264 p.

Luo, X. R., 1999, Fault opening and the transit variation of

temperature and pressure in formations: mathematical modeling (in Chinese): Oil and Gas Geology, v. 20, p. 1–6.

Luo, X. R., and G. Vasseur, 1992, Contributions of compaction and aquathermal pressuring to geopressure and the influence of environmental conditions: AAPG Bulletin, v. 76, p. 1550–1559.

Luo, X. R., and G. Vasseur, 1996, Geopressuring mechanism of organic matter cracking: numerical modeling: AAPG Bulletin, v. 80, p. 856–874.

Luo, X. R., and G. Vasseur, 1997, Sealing efficiency of shales: Terra Nova, v. 9, p. 71–74.

Luo, X. R., F. Brigaud, and G. Vasseur, 1993, Compaction coefficient of argillaceous sediments: its implications, significance and determination, *in* A. G. Doré, J. H. Augustson, C. Hermanrud, D. J. Stewart, and Ø. Sylta, eds., Basin modelling, advances and applications: Norwegian Petroleum Society Special Publication 3: Amsterdam, Elsevier, p. 321–332.

Luo, X. R., J. H. Yang, and Z. F. Wang, 2000, The overpressuring mechanisms in aquifers and pressure prediction in basins (in Chinese): Geological Review, v. 46, p. 22–31.

Magara, K., 1978, Compaction and fluid migration, practical petroleum geology: Amsterdam, Elsevier, 319 p.

Nunn, J. A., 1996, Buoyancy-driven propagation of isolated fluid-filled fractures: implications for fluid transport in Gulf of Mexico geopressured sediments: Journal of Geophysical Research, v. 101, p. 2963–2970.

Osborne, M. J., and R. E. Swarbrick, 1997, Mechanisms for generating overpressure in sedimentary basins: a reevaluation: AAPG Bulletin, v. 81, p. 1023–1041.

Roberts, S. J., and J. A. Nunn, 1995, Episodic fluid expulsion from geopressured sediments: Marine and Petroleum Geology, v. 12, p. 195–204.

Shi, Y. L., and C. Y. Wang, 1986, Pore pressure generation in sedimentary basins: overloading versus aquathermal: Journal of Geophysical Research, v. 91, p. 2153–2162.

Smith, J. E., 1971, The dynamics of shale compaction and evolution of pore-fluid pressures: Mathematical Geology, v. 3, p. 239–263.

Snow, D. T., 1969, Anisotopic permeability of fractured media: Water Resource Research, v. 5, p. 1273–1289.

Surdam, R. C., Z. S. Jiao, and R. S. Martinsen, 1994, The regional pressure regime in cretaceous sandstones and shales in the Powder River basin, *in* P. Ortoleva, Basin compartments and seals: AAPG Memoir 61, p. 213–234.

Swarbrick, R. E., and M. Osborne, 1996, The nature and diversity of pressure transition zones: Petroleum Geoscience, v. 2, p. 111–116.

Tissot, B., and J. Espitalié, 1975, L'évolution thermique de la matière organique des sédiments: applications d'une simulation mathématique: Revue de l'Institut Français du Pétrole, v. 30, p. 743–777.

Turcotte, D. L., and G. Schubert, 1982, Geodynamics— applications of continuum physics to geological problems: New York, Wiley, 450 p.

Ungerer, P., F. Bessis, Y. Chenet, B. Durand, E. Nogaret, A. Chiarelli, J. L. Oudin, and J. K. Perrin, 1984, Geological and geochemical models in oil exploration: principles and practical examples, *in* G. Demaison, ed., Petroleum geochemistry and basin evaluation: AAPG Memoir 35, p. 53–57.

Ungerer, P., J. Burrus, B. Doligez, Y. Chenet, and F. Bessis, 1990, Basin evaluation by integrated two-dimensional modeling of heat transfer, fluid flow, hydrocarbon generation, and migration: AAPG Bulletin, v. 74, p. 309–335.

Wang, L. S., 2000, The origin and evolution of the Yinggehai Basin (abs. in Chinese): Meeting on new developments in petroleum basin studies: Chinese Association of Petroleum Researchers, Jiujiang, May 12–14, 2000.

Wang, C. Y., and X. N. Xie, 1998, Hydrofracturing and episodic fluid flow in shale-rich basins— a numerical study: AAPG Bulletin, v. 82, p. 1857–1869.

Wyllie, M. R. J., A. R. Gregory, and G. H. F. Gardner, 1958, An experimental investigation of factors affecting elastic wave velocities in porous media: Geophysics, v. 23, p. 459–493.

Xie, X. N., S. T. Li, W. L. Dong, and Z. L. Hu, 2001, Evidence for episodic expulsion of hot fluids along faults near diapiric structures of the Yinggehai Basin, South China Sea: Marine and Petroleum Geology, v. 18, p. 715–728.

Zhang, Q. M., and Q. X. Zhang, 1993, A distinctive hydrocarbon basin-Yinggehai Basin (in Chinese), *in* Q. M. Zhang, ed., A collection on petroleum geology of the Yinggehai Basin, South China: Beijing, Seismology Press, p. 10–17.

Zhang, Q. M., F. N. Liu, and J. H. Yang, 1996, Overpressure systems and petroleum accumulation in the Yinggehai Basin (in Chinese): Chinese Marine Oil and Gas (Geology), v. 10, p. 65–75.

Zhang, F. Q., Z. L. Wang, Y. S. Wu, J. H. Yang, and X. R. Luo, 2002, The methods to reduce the geological influences on compaction curves: taking the Yinggehai Basin as an example (in Chinese): Acta Sedimentologica Sinica, v. 20, p. 326–331.